Journal of Innovative Optical Health Sciences
Vol. 7, No. 3 (2014) 1450008 (9 pages)

DOI: 10.1142/S1793545814500084

World Scientific
www.worldscientific.com

Sparse reconstruction for fluorescence molecular tomography via a fast iterative algorithm

Jingjing Yu*,‡, Jingxing Cheng†, Yuqing Hou† and Xiaowei He†
*School of Physics and Information Technology
Shaanxi Normal University
Xi'an 710062, P. R. China
†School of Information Sciences and Technology
Northwest University
Xi'an 710069, P. R. China
‡yujj@snnu.edu.cn

Received 7 August 2013
Accepted 3 November 2013
Published 17 December 2013

Fluorescence molecular tomography (FMT) is a fast-developing optical imaging modality that has great potential in early diagnosis of disease and drugs development. However, reconstruction algorithms have to address a highly ill-posed problem to fulfill 3D reconstruction in FMT. In this contribution, we propose an efficient iterative algorithm to solve the large-scale reconstruction problem, in which the sparsity of fluorescent targets is taken as useful *a priori* information in designing the reconstruction algorithm. In the implementation, a fast sparse approximation scheme combined with a stage-wise learning strategy enable the algorithm to deal with the ill-posed inverse problem at reduced computational costs. We validate the proposed fast iterative method with numerical simulation on a digital mouse model. Experimental results demonstrate that our method is robust for different finite element meshes and different Poisson noise levels.

Keywords: Fluorescence molecular tomography; sparse regularization; reconstruction algorithm; least absolute shrinkage and selection operator.

1. Introduction

Fluorescence molecular tomography (FMT) is a promising imaging modality that allows detailed investigations of biological processes, disease progression, and response to therapy at a molecular level within small animals. Compared with plane fluorescence imaging, FMT provides more quantitative and accurate information of spatial location and strength

of fluorescent sources (usually fluorescent probe tagging the molecule of interest). It has recently gained much attention in the field of pre-clinical studies, such as drug development, early cancer detection and cell-based therapy.[1–6]

Methodologies or schema for quantitative image reconstruction is the key to the further advancement of FMT. In this paper, we focus on the inverse problem of FMT based on continuous wave fluorescence measurements, i.e., recovery of the 3D distribution of the interior fluorescent source from measurements at the tissue surface based on a photons propagating model.

Due to high degrees of absorption and scattering of photons propagating through biological tissue, the inverse problem of FMT is inherently illposed. Consequently, various regularization strategies become indispensable for the inverse algorithm to obtain stable solution.[7–9] In addition, *a priori* knowledge regarding solution is usually incorporated into image reconstruction to play an important role in improving the solution quality, e.g., anatomical information,[10–12] local smoothness,[13] or sparsity.[14,15]

To solve the inverse problem, prior knowledge regarding the solution usually presents in the form of a regularizer or a penalty term in the objective function, such as Tikhonov regularization, l_1 regularization and total variation (TV) regularization. Typically, the biological mechanisms are locally concentrated within specific areas of interest, which means the fluorescence-labeled targets present a sparse distribution in the volume or the solutions only have a few nonzero coefficients. The l_1 norm is a widely used sparsity-inducing norm and recent researches have witnessed that l_1 regularization is a preferable choice for sparse images reconstruction of FMT.[16–22]

In this contribution, the inverse problem of FMT is formulated into a least absolute shrinkage and selection operator (LASSO) problem by l_1 regularization and a fast iterative algorithm is developed to reconstruct the fluorophore distribution. Simulations on 3D digital mouse model are performed to evaluate the proposed method.

2. Method

2.1. *Inverse model*

In continuous wave FMT, the distribution of the fluorophore is recovered from the steady state surface measurements. With the diffusion approximation, the photons propagation through tissue can be described by a set of coupled partial differential equations.[19–22] By solving the diffusion equation numerically using the finite elements method,[23–25] we can build a linear relationship between the unknown fluorescence target x and the measured surface fluorescence data b:

$$Ax = b, \tag{1}$$

where $A \in R^{m\times n}$ is the system matrix. Typically, A for FMT is a large size rank-deficient matrix, therefore constraints are necessary to distinguish the meaningful solution from an infinite number of solutions. We take the sparsity as a constraint and formulate the inverse problem of FMT into an l_1-norm regularized optimization problem:

$$\min_X\{L(x) = \|Ax - b\|_2 + \lambda\|x\|_1\}. \tag{2}$$

The problem in (2) is a LASSO problem,[26] also known as basis pursuit.[27] We proposed an efficient iterative algorithm for solving such optimization problem in (2),[28] which will be referred to as stagewise fast LASSO (SwF-LASSO) in the following section. Here, SwF-LASSO is used to solve the convex optimization problem for FMT.

2.2. *Stagewise fast LASSO*

Obviously, the objective function in (2) is convex but not differentiable. We define some notations to simplify the objective function. Let the residual vector be $r(x) = Ax - b$, where $r(x) = (r_1(x), \ldots, r_m(x))^{\mathrm{T}}$. Let $\omega = (\omega_1, \ldots, \omega_n)^{\mathrm{T}}$, $\omega_i = \begin{cases} \mathrm{sign}(x_i), & x_i \neq 0 \\ \alpha_i \in \{-1, 1\}, & x_i = 0 \end{cases}$, $i = 1, \ldots, n$. Define the sign vector $\mathbf{s}(x) = (s_1(x), \ldots, s_m(x))^{\mathrm{T}}$ by

$$s_i(x) = \begin{cases} 1 & 0 < r_i(x) < \infty \\ -1 & -\infty < r_i(x) < 0 \\ 0 & \text{otherwise} \end{cases}. \tag{3}$$

Then the objective function can be reformulated into

$$\min_X\{L(x) = x^{\mathrm{T}}A^{\mathrm{T}}Ax - 2((A)^{\mathrm{T}}b - \lambda\omega^{\mathrm{T}}/2)x\}. \tag{4}$$

By setting the deviation of (4) to zero, it is easy to derive the solution of (2) that takes the form of:

$$\hat{x} = (A^{\mathrm{T}}A)^{-1}(A^{\mathrm{T}}b - \lambda\omega/2). \tag{5}$$

However, the solution cannot be determined directly with (5) because ω depends on x. Moreover, the matrix inversion in (5) is a time-consuming operation for a large-size system matrix A. To avoid matrix inversion, we employ a greedy scheme to solve (4) efficiently, which is inspired by the fast sparse approximation for least squares support vector machine.[29,30] In the implementation, we regard matrix A as a basis function dictionary, i.e., $A = [a_1, a_2, \ldots, a_n]$ is the $m \times n$ dictionary. Two index sets, S and P, are used in the proposed algorithm. The algorithm works by initializing index set P empty and $S = \{1, 2, \ldots, n\}$. SwF-LASSO iteratively builds the decision function by adding several basis functions (columns of A) and updates the parameters until the given stopping criterion is satisfied. Once some basis functions are picked from the dictionary A, the corresponding indices will be eliminated from S and added to set P.

We assume that the index set P contains n_p elements at the nth iteration, which means n_p basis functions or columns of A have been selected to form a $m \times n_p$ sub-matrix of A, denoted by A_P. The components of x corresponding to A_P are denoted by vector x_P and the other components are set to zero. Let us now illustrate how to compute the inverse matrix and update the solution iteratively. Let $Q^n = (A_P^{\mathrm{T}} A_P)^{-1}$. Given that other k basis functions are selected at the $(n+1)$th iteration and be ranged in a sub-matrix A_k. Then

$$\begin{aligned} Q^{n+1} &= \left(\begin{pmatrix} A_P^{\mathrm{T}} \\ A_K^{\mathrm{T}} \end{pmatrix} (A_P \quad A_K) \right)^{-1} \\ &= \begin{pmatrix} A_P^{\mathrm{T}} A_P & A_P^{\mathrm{T}} A_K \\ A_K^{\mathrm{T}} A_P & A_K^{\mathrm{T}} A_K \end{pmatrix}^{-1} \\ &= \begin{pmatrix} (Q^n)^{-1} & A_P^{\mathrm{T}} A_K \\ A_K^{\mathrm{T}} A_P & A_K^{\mathrm{T}} A_K \end{pmatrix}^{-1} \\ &= \begin{pmatrix} Q^n & \mathbf{0} \\ \mathbf{0^T} & 0 \end{pmatrix} + \eta \begin{pmatrix} \rho \\ -1 \end{pmatrix} (\rho^{\mathrm{T}} - 1)(Q^n)^{-1}, \quad (6) \end{aligned}$$

where $\rho = Q^n A_P^{\mathrm{T}} A_K$, $\eta = (A_K^{\mathrm{T}} A_K - A_K^{\mathrm{T}} A_P \rho)^{-1}$. Combing with (5), the iterative formula for the solution x is obtained accordingly

$$\begin{aligned} (x^{n+1}) &= \begin{pmatrix} x_P^{n+1} \\ x_K^{n+1} \end{pmatrix} = Q^{n+1} \begin{pmatrix} A_P^{\mathrm{T}} b - \lambda \omega_P / 2 \\ A_K^{\mathrm{T}} b - \lambda \omega_K / 2 \end{pmatrix} \\ &= \begin{pmatrix} Q^n & \mathbf{0} \\ \mathbf{0^T} & 0 \end{pmatrix} \begin{pmatrix} A_P^{\mathrm{T}} b - \lambda \omega_P / 2 \\ A_K^{\mathrm{T}} b - \lambda \omega_K / 2 \end{pmatrix} \\ &\quad + \eta \begin{pmatrix} \rho \\ -1 \end{pmatrix} (\rho^{\mathrm{T}} - 1) \begin{pmatrix} A_P^{\mathrm{T}} b - \lambda \omega_P / 2 \\ A_K^{\mathrm{T}} b - \lambda \omega_K / 2 \end{pmatrix} \\ &= \begin{pmatrix} x_P^n \\ \mathbf{0} \end{pmatrix} + \begin{pmatrix} \rho \eta \Delta \\ -\eta \Delta \end{pmatrix}, \quad (7) \end{aligned}$$

where $\Delta = \rho^{\mathrm{T}}(A_P^{\mathrm{T}} b - \lambda \omega_P / 2) - A_K^{\mathrm{T}} b + \lambda \omega_K / 2$.

In fact, the optimization problem in (4) is solved with a greedy scheme, i.e., SwF-LASSO iteratively builds the decision function by adding several basis functions (columns of A). The criterion for selecting basis functions is to maximize the descending in the objective function caused by adding basis functions to the model. For example, given $i \in S$, $\Delta L_i^{n+1} = L_i^{n+1} - L^n$ denotes the descent caused by adding the ith basis function. Here,

$$\begin{aligned} \Delta L_i^{n+1} &= L_i^{n+1} - L^n = x_i^2 a_i^{\mathrm{T}} a_i + 2 x_i \\ &\quad \times \left((a_i^{\mathrm{T}} A_P x_P) - \left(b^{\mathrm{T}} a_i - \frac{\lambda}{2} \omega_i \right) \right). \quad (8) \end{aligned}$$

So the selection of basis functions is equivalent to the following sub-problem:

$$\min_{x_i} \{ a_i^{\mathrm{T}} a_i x_i^2 + 2 q_i^n x_i \}, \quad (9)$$

where

$$q_i^n = \begin{cases} -(b^{\mathrm{T}} a_i - \lambda \omega_i / 2) & n = 0 \\ a_i^{\mathrm{T}} A_P x_P - (b^{\mathrm{T}} a_i - \lambda \omega_i / 2) & n > 0 \end{cases}. \quad (10)$$

It is easy to compute that the optimal solution of (9) is

$$\Delta L_i^{n+1} = -(q_i^n)^2 / a_i^{\mathrm{T}} a_i. \quad (11)$$

To accelerate the convergence of the algorithm, a stage-wise learning strategy is adopted to select several basis functions at a time. The stage-wise size is adaptively determined based on γ threshold. Specifically, γ threshold is computed by

$$\gamma = \sqrt{\sum_{i \in S} (\Delta L_i^{n+1})^2 / |S|}, \quad (12)$$

where $|S|$ represents the cardinality of index set S. According to the stage-wise strategy, the basis functions to be selected are the columns indexed by the elements of

$$K^{n+1} = \left\{ i | \ \nu > |\Delta L_i^{n+1}| > c \cdot \gamma, i \in S \right\}, \quad (13)$$

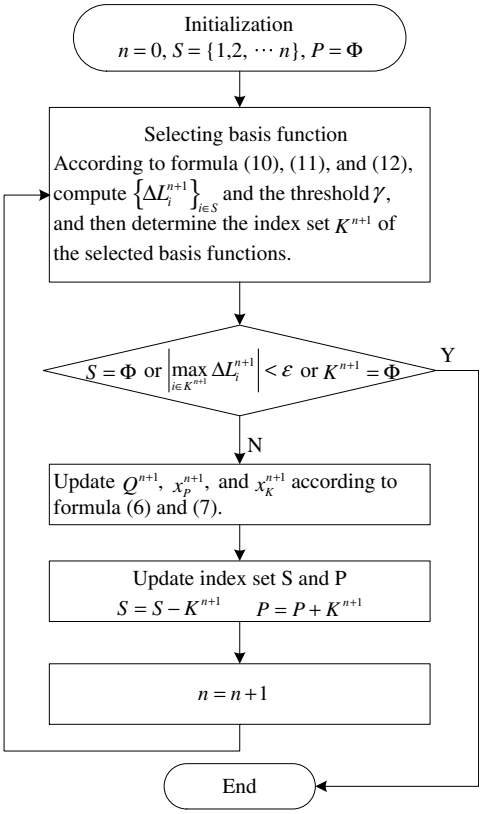

Fig. 1. Flowchart of StF-LASSO algorithm.

where $|\Delta L_i^{n+1}|$ denotes the absolute value of ΔL_i^{n+1}. ν and c are two positive constants and their values control the stage-wise size. In the experiments, c ranges from 1 to 3.

The iterations continue until one of the following stopping criteria is met: (1) The index set S is empty; (2) K^{n+1} is empty; (3) $|\max_{i\in K^{n+1}} \Delta L_i^{n+1}| < \varepsilon$. If algorithm stops at the kth iteration, then the sparse solution of (2) can be approximated by x^k.

The flowchart of StF-LASSO algorithm is illustrated in Fig. 1.

3. Experiments and Results

In this section, the performance of the presented SwF-LASSO approach is experimentally verified and is compared with IVTCG[19] and StOMP.[21] All the experiments are performed on the same 3D digital mouse model.[31] We obtained anatomical information from the mouse model of CT and cryosection data, as shown in Fig. 2(a). The torso section of the mouse atlas with a height of 35 mm is the volume to investigate. A total of 18 point sources were placed around the surface for

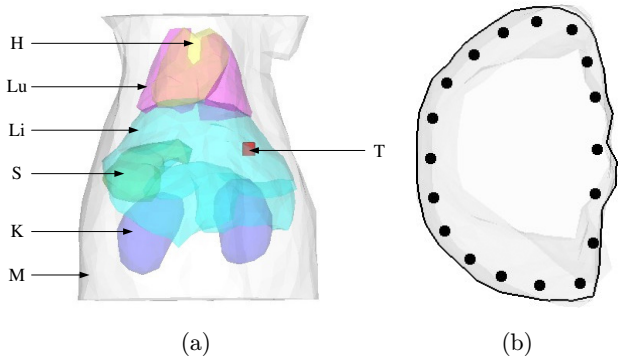

Fig. 2. (a) 3D digital mouse model consisting of heart (H), lungs (Lu), muscle (M), liver (Li), kidneys (K), stomach (S), muscle (M) and target (T). (b) A total of 18 excitation sources placed around the surface at $z = 16.4$ mm plane.

Table 1. Optical properties for the main organs region of 3D mouse model.

Material	μ_{ax} (mm^{-1})	μ'_{sx} (mm^{-1})	μ_{am} (mm^{-1})	μ'_{sm} (mm^{-1})
Heart	0.0083	1.01	0.0104	0.99
Lungs	0.0133	1.97	0.0203	1.95
Liver	0.0329	0.70	0.0176	0.65
Stomach	0.0114	1.74	0.0070	1.36
Kidneys	0.0660	2.25	0.0380	2.02

excitation as shown in Fig. 2(b). The optical properties of different main organs are listed in Table 1.[19]

The measurements used in the numerical experiments were obtained by solving the forward model with FEM. To do this, the torso mouse model was discretized into 24,906 nodes and 132,202 tetrahedral elements. But in the reconstruction process, the mesh consisted of 2604 nodes and 12,376 tetrahedral elements, and the maximum and minimum mesh sizes are 3.2 and 0.2 mm, respectively. Swf-Lasso, IVTCG and StOMP are separately employed to solve the FMT inverse problem in (2). Reconstruction performance was evaluated in terms of location error, fluorescent yield and runtime. The quantitative comparison is listed in Table 2. Figure 3 shows the results of the above three methods for single target reconstruction.

From Table 2, we can find that the presented Swf-Lasso algorithm stand as a comparison with StOMP and perform slightly better than IVTCG in the single target setting. The source centers reconstructed by the three methods are identical and the

Table 2. Result for single target reconstruction.

Method	Position (mm)	Location error (mm)	Fluorescent yield (mm^{-1})	Time (s)
SwF-LASSO	**11.8,6.3,16.0**	**0.40**	**0.018**	**0.87**
IVTCG	11.8,6.3,16.0	0.40	0.005	19.37
StOMP	11.8,6.3,16.0	0.40	0.026	0.82

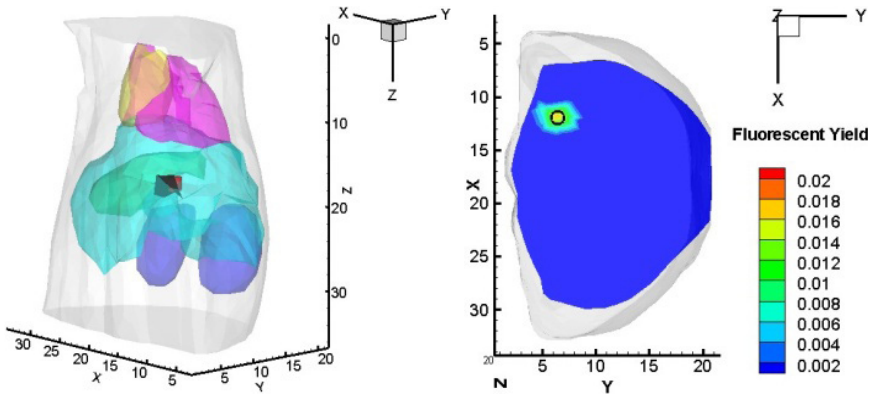

(a) Swf-Lasso

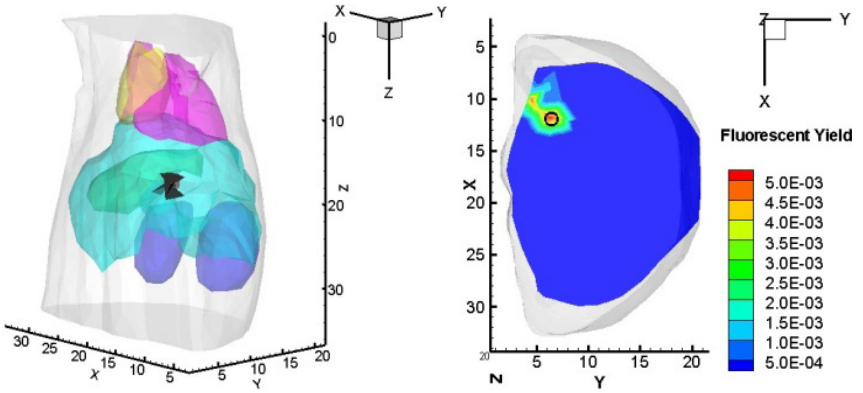

(b) IVTCG

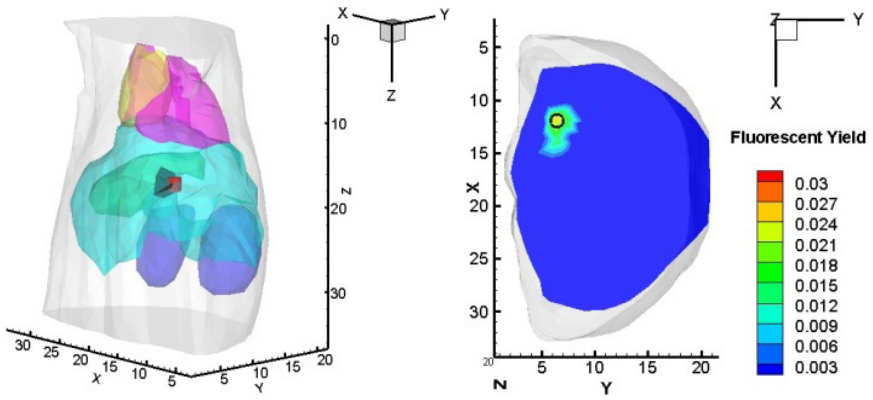

(c) StOMP

Fig. 3. Comparison of reconstruction results for single target, a red cylinder represents the actual source and the black region means the position of reconstruction.

location error is 0.40 mm. In fact, the reconstructed source center is also the nearest node to the actual source, which means all the three algorithms locate the target accurately. As for the computing time, Swf-Lasso and StOMP run faster than IVTCG.

3.1. *Reconstruction of double targets*

In the case of double targets reconstruction, two cylinder fluorescent targets of 1.6 mm high by 0.8 mm radius were set in the liver. The center of these targets located in (11.9, 6.4, 16.4 mm) and (11.9, 10.9, 16.4 mm), and the actual fluorescent yield is 0.05 mm^{-1}. A total of 18 point sources were placed around the surface for excitation. The comparisons of these methods are shown in Table 3 and Fig. 4.

The quantitative results in Table 3 demonstrate that our algorithm is better than the compared methods. Although, SwF-LASSO runs slightly slower than StOMP, it yields more accurate reconstruction. The location errors for the two targets by our method are 0.60 and 1.03 mm, respectively. In contrast, one of the reconstructed sources with IVTCG and StOMP method deviated from the actual target. Meanwhile, our proposed method obtains satisfied fluorescent yield which is near the actual value.

3.2. *Stability analysis*

In this part, three groups of experiments are presented to evaluate the robustness and stability of our algorithm.

Firstly, we added different levels (0%, 10%, 20%, 40%) of Poisson noise to boundary measurements. We implemented 60 independent reconstructions for each noise level. The impacts of noise on reconstruction results are shown in Table 4.

As shown in Table 4, for all the noise levels considered, the source locations are identical to that of without noise. Furthermore, we find that the reconstructed power varies very slightly with the increase of noise level, and the maximum deviation of the power occurs at 30% noise level, which possess a maximum 9.4% deviation to the actual power.

Table 3. Results for double targets reconstruction.

Method	Position center (mm)	Location error (mm)	Fluorescent yield (mm^{-1})	Time (s)
SwF-LASSO	**11.7,10.4,16.5**	**0.60**	**0.045**	**0.95**
	11.1,6.8,16.9	**1.03**	**0.037**	
IVTCG	11.7,10.4,16.5	0.60	0.018	24.66
	10.3,5.3,16.4	1.26	0.010	
StOMP	11.7,10.4,16.5	0.60	0.022	0.87
	11.3,5.3,16.4	1.26	0.010	

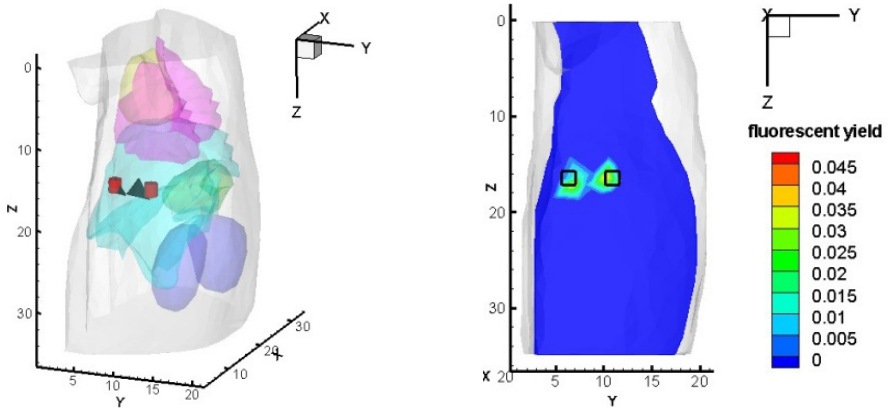

(a) Swf-Lasso

Fig. 4. Reconstruction results for double targets, two red cylinders represent the actual sources and the black region means the position of reconstruction.

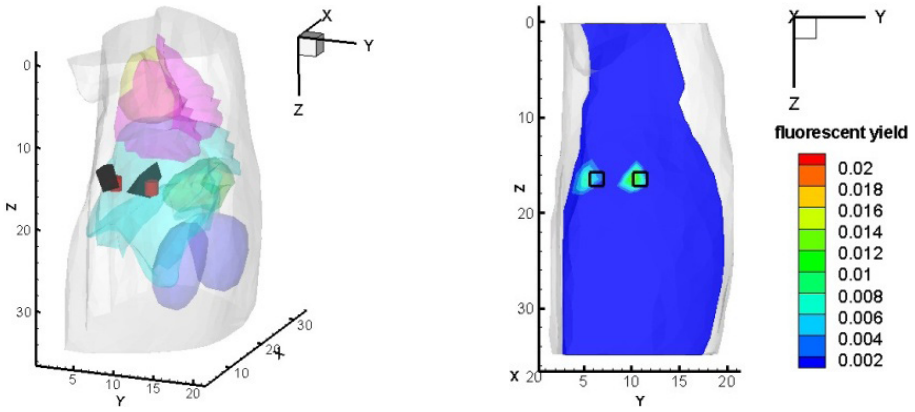

(b) IVTCG

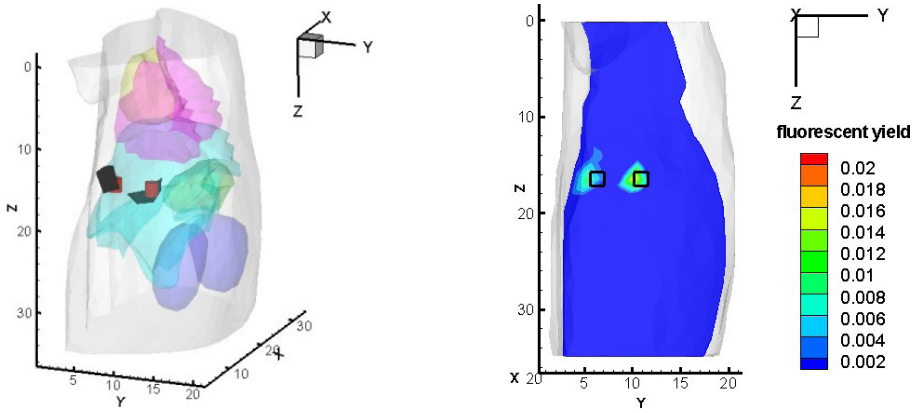

(c) StOMP

Fig. 4. (*Continued*)

Table 4. Impact of Poisson noise on the proposed method.

Noise level	Position center (mm)	Location error (mm)	Fluorescent yield (mm^{-1})
0%	11.8,6.3,16.0	0.40	0.0182 ± 0.0012
10%	11.8,6.3,16.0	0.40	0.0182 ± 0.0010
20%	11.8,6.3,16.0	0.40	0.0183 ± 0.0016
40%	11.8,6.3,16.0	0.40	0.0184 ± 0.0021

As for location error, the proposed algorithm obtained the same best results under different noise levels. From the view of fluorescent yield, the means of results for different noise levels have a slight fluctuation. Therefore, we can make a conclusion that our proposed method is robust for Poisson noise.

Secondly, we changed different meshes for reconstruction to evaluate the stability of our method. We utilized three different meshes to reconstruct single target separately, i.e., the model were discretized into 1349 nodes and 6036 tetrahedral elements, 2604 nodes and 12,376 tetrahedral elements, 3620 nodes and 17,504 tetrahedral elements, respectively. We computed that the location errors for the best point of these meshes were 1.14, 0.40, 1.22 mm, respectively. Meanwhile, the corresponding initial fluorescent yield on different meshes is $0.05\,mm^{-1}$. The experimental results on different meshes are shown in Table 5. It is obviously shown in Table 5 that the points of our reconstruction are the best points, respectively on different mesh levels. In conclusion, we can say that our algorithm is stable for different meshes.

At last, we reconstructed the single target on the condition of decreasing excitation sources. Based on the single target experiments, we decrease the number of excitation sources from 18 to 12, 9 and 6, separately. The results of this group experiments are shown in Table 6.

Table 5. Impact of different meshes on the proposed method.

Size of matrix A	Position center (mm)	Location error (mm)	Fluorescent yield (mm^{-1})
2506*1349	12.4,7.4,16.2	1.14(1.14)	0.091(0.05)
3938*2604	11.8,6.3,16.0	0.40(0.40)	0.0182(0.05)
5325*3620	11.3,5.3,16.3	1.22(1.22)	0.0101(0.05)

Table 6. Impact of different excitation sources on the proposed method.

Number of excitation sources	Position center (mm)	Location error (mm)	Fluorescent yield (mm^{-1})
18	11.8,6.3,16.0	0.40	0.18
12	11.8,6.3,16.0	0.40	0.13
9	13.0,6.8,16.6	1.22	0.08
6	13.0,6.8,16.6	1.22	0.07

From Table 6, it is shown that we obtain satisfied result in 18 excitation sources and 12 excitation sources. However, when we decrease them to half or one third of full number, the position of reconstruction deviates from the best point. Moreover, the fluorescent yield declines along with decreasing excitation source.

4. Discussion and Conclusion

In this paper, we propose an efficient reconstruction algorithm for inverse problem of FMT. Considering sparse distribution of fluorescent target in the imaging domain, sparsity regularization is employed to deal with the ill-posedness of tomographic fluorescence imaging problem. To solve the l_1-norm regularized objective functions efficiently, a fast iterative algorithm is developed to find stable approximate solution. Numerical experiments with 3D digital mouse model verify that our proposed algorithm is feasible, stable and efficient.

With respect to quantitative indexes and visual qualities of the experimental results, the proposed SwF-LASSO algorithm performs comparable to StOMP and better than the IVTCG in single target reconstruction. Nevertheless, the presented algorithm performs best in double targets reconstruction. The stability tests further demonstrate that the SwF-LASSO algorithm is stable and robust to measure noise and mesh discretization. In addition, SwF-LASSO yields satisfactory reconstruction when we decrease the number of excitation source from 18 to 12, but the results experience a noticeable decline in quality when the number further decreases. Consequently, the number of excitation sources has a degree of impact on reconstruction results.

In conclusion, the presented SwF-LASSO algorithm is a stable and efficient iterative algorithm for tomographic fluorescence imaging problem, and the *in vivo* evaluation will be reported in future.

Acknowledgment

This work is supported by the National Natural Science Foundation of China (Grant No. 61372046), the Research Fund for the Doctoral Program of Higher Education of China (New Teachers) (Grant No. 20116101120018), the China Postdoctoral Science Foundation Funded Project (Grant Nos. 2011M501467 and 2012T50814), the Natural Science Basic Research Plan in Shaanxi Province of China (Grant No. 2011JQ1006), the Fundamental Research Funds for the Central Universities (Grant No. GK201302007), Science and Technology Plan Program in Shaanxi Province of China (Grant Nos. 2012 KJXX-29 and 2013K12-20-12), the Science and Technology Plan Program in Xi'an of China (Grant No. CXY1348(2)).

References

1. V. Ntziachristos, J. Ripoll, L. V. Wang, R. Weissleder, "Looking and listening to light: The evolution of whole-body photonic imaging," *Nat. Biotechnol.* **23**(3), 313–320 (2005).
2. J. Tian, Bai, X. Yan *et al.*, "Multimodality molecular imaging: Improving image quality," *IEEE Eng. Med. Biol. Mag.* **27**(5), 48–57 (2008).
3. R. Weissleder, U. Mahmood, "Molecular imaging," *Radiology* **219**(2), 316–333 (2001).
4. M. J. Niedre *et al.*, "Early photon tomography allows fluorescence detection of lung carcinomas and disease progression in mice in vivo," *Proc. Natl. Acad. Sci. USA* **105**(49), 19126–19131 (2008).
5. J. K. Willmann, N. van Bruggen, L. M. Dinkelborg, S. S. Gambhir, "Molecular imaging in drug development," *Nat. Rev. Drug Discov.* **7**(7), 591–607, (2008).
6. S. R. Arridge, "Optical tomography in medical imaging," *Inverse Probl.* **15**, R41–R93 (1999).

7. Y. Tan, H. Jiang, "DOT guided fluorescence molecular tomography of arbitrarily shaped objects," *Med. Phys.* **35**, 5703–5707 (2008).
8. X. Wang, C. Xu, J. Bai *et al.*, "A hybrid reconstruction algorithm for fluorescence tomography using Kirchhoff approximation and finite element method," *Med. Biol. Eng.* **51**, 7–17 (2013).
9. J.-C. Baritaux, K. Hassler, M. Unser, "An efficient numerical method for general Lp regularization in fluorescence molecular tomography," *IEEE Trans. Med. Imaging* **29**(4) (2010).
10. Y. Lin, H. Yan, O. Nalcioglu, G. Gulsen, "Quantitative fluorescence tomography with functional and structural a priori information," *Appl. Opt.* **48**, 1328–1336 (2009).
11. S. C. Davis, H. Dehghani, J. Wang, S. Jiang, B. W. Pogue, K. D. Paulsen, "Image-guided diffuse optical fluorescence tomography implemented with Laplacian-type regularization," *Opt. Express* **15**, 4066–4082 (2007).
12. D. Hyde, E. L. Miller, D. H. Brooks, V. Ntziachristos, "Data specific spatially varying regularization for multi-modal fluorescence molecular tomography," *IEEE Trans. Med. Imaging.* **29**, 365–374 (2010).
13. M. Li, X. Cao, F. Liu, B. Zhang, J. Luo, J. Bai, "Reconstruction of fluorescence molecular tomography using a neighborhood regularization," *IEEE Trans. Biomed. Eng.* **59**, 1799–1803 (2012).
14. J. Dutta, S. Ahn, C. Li, S. R. Cherry, R. M. Leahy, "JointL1 and total variation regularization for fluorescence molecular tomography," *Phys. Med. Biol*, **57**, 1459–1476 (2012).
15. P. Mohajerani, A. A. Eftekhar, J. Huang, A. Adibi, "Optimal sparse solution for fluorescent diffuse optical tomography: Theory and phantom experimental results," *Appl. Opt.* **46**, 1679–1685 (2007).
16. D. Han, J. Tian, S. Zhu, J. Feng, C. Qin, B. Zhang, X. Yang, "A fast reconstruction algorithm for fluorescence molecular tomography with sparsity regularization," *Opt. Express.* **18**, 8630–8646 (2010).
17. D. Wang, X. Song, J. Bai, "Adaptive-mesh-based algorithm for fluorescence molecular tomography using an analytical solution," *Opt. Express* **15**(15), 9722–9730 (2007).
18. H. Gao, H. Zhao, "Multilevel bioluminescence tomography based on radiative transfer equation. Part 2: Total variation and L1 data fidelity," *Opt. Express* **18**(3), 2894–2912 (2010).
19. H. Yi, D. Chen, X. Qu, K. Peng, X. Chen, Y. Zhou, J. Tian, L. Jimin, "Multilevel, hybrid regularization method for reconstruction of fluorescent molecular tomography," *Appl. Opt.* **51**(7), 975–986 (2012).
20. X. He, J. Liang, X. Wang *et al.*, "Sparse reconstruction for quantitative bioluminescence tomography based on the incomplete variables truncated conjugate gradient method," *Opt. Express* **18**(24), 24825–24841 (2010).
21. D. Han, X. Yang, K. Liu, B. Zhang, X. Ma, J. Tian, "Efficient reconstruction method for L1 regularization in fluorescence molecular tomography," *Appl. Opt.* **49**(36), 6930–6937 (2010).
22. H. Yi, D. Chen, W. Li, S. Zhou, M. Ning, S. Zhu, J. Tian, J. Liang, "Normalized born approximation-based two-stage reconstruction algorithm for quantitative fluorescence molecular tomography," *J. Electrical Comput. Eng.* **2012**, 838967 (2012).
23. M. Schweiger, S. R. Arridge, M. Hiraoka, D. T. Delpy, "The finite element method for the propagation of light in scattering media: Boundary and source conditions," *Med. Phys.* **22**, 1779–1792 (1995).
24. D. Wang, X. Liu, Y. Chen, J. Bai, "A novel finite-element based algorithm for fluorescence molecular tomography of heterogeneous media," *IEEE Trans. Inf. Technol. Biomed.* **13**, 766–773 (2009).
25. W. Cong, G. Wang, "A finite-element-based reconstruction method for 3D fluorescence tomography," *Opt. Express* **13**, 9847–9857 (2005).
26. R. Tibshirani, "Regression shrinkage and selection via the LASSO," *J. R. Stat. Soc.* **58**, 267–288 (1996).
27. S. S. Chen, D. L. Donoho, M. A. Saunders, "Atomic decomposition by basis pursuit," *J. Sci. Comput.* **20**(1), 33–61 (1998).
28. J. Yu, F. Liu, J. Wu, L. Jiao, X. He, "Fast source reconstruction for bioluminescence tomography based on sparse regularization," *IEEE Trans. Biomed. Eng.* **57**(10), 2583–2586 (2010).
29. J. A. K. Suykens, L. Lukas, J. Vandewalle, "Sparse approximation using least squares support vector machines," *Circuits Sys.* **2**, 757–760 (2000).
30. L. Jiao, L. Bo, L. Wang, "Fast sparse approximation for least square support vector machine," *IEEE Trans. Neural Netw.* **18**(3), 685–697 (2007).
31. B. Dogdas, D. Stout, A. F. Chatziioannou, R. M. Leahy, "Digimouse: A 3D whole body mouse atlas from CT and cryosection data," *Phys. Med. Biol.* **52**, 577–587 (2007).